VIP Metals in Medicine Very Important Paper

How to cite: *Angew. Chem. Int. Ed.* **2022,** *61,* e202209136
International Edition: doi.org/10.1002/anie.202209136
German Edition: doi.org/10.1002/ange.202209136

An Anticancer Rhenium Tricarbonyl Targets Fe–S Cluster Biogenesis in Ovarian Cancer Cells

Benjamin Neuditschko[+], A. Paden King[+], Zhouyang Huang, Lukas Janker, Andrea Bileck, Yasmin Borutzki, Sierra C. Marker, Christopher Gerner, Justin J. Wilson, and Samuel M. Meier-Menches**

Abstract: Target identification remains a critical challenge in inorganic drug discovery to deconvolute potential polypharmacology. Herein, we describe an improved approach to prioritize candidate protein targets based on a combination of dose-dependent chemoproteomics and treatment effects in living cancer cells for the rhenium tricarbonyl compound TRIP. Chemoproteomics revealed 89 distinct dose-dependent targets with concentrations of competitive saturation between 0.1 and 32 μM despite the broad proteotoxic effects of TRIP. Target-response networks revealed two highly probable targets of which the Fe–S cluster biogenesis factor NUBP2 was competitively saturated by free TRIP at nanomolar concentrations. Importantly, TRIP treatment led to a down-regulation of Fe–S cluster containing proteins and upregulated ferritin. Fe–S cluster depletion was further verified by assessing mitochondrial bioenergetics. Consequently, TRIP emerges as a first-in-class modulator of the scaffold protein NUBP2, which disturbs Fe–S cluster biogenesis at sub-cytotoxic concentrations in ovarian cancer cells.

Introduction

Chemical proteomics based on affinity interactions enables identifying targets of metal-based drug candidates in cellular systems.[1] Such target identification approaches were considerably improved and diversified over the past years and now include a broad range of chemical and thermal labelling strategies.[2] Chemical proteomics and photoaffinity labelling rely on synthetic modifications of drug candidates that might impact on their accumulation, distribution and potential target interactions. Nonetheless, these approaches successfully revealed the target landscape of several metal-based drug candidates because of their enrichment efficiency.[3] A biotin modification was used to immobilize a ruthenium-(arene) derivative of plecstatin-1, which was found to be a highly selective modulator of the scaffold protein plectin.[4] Recent findings proved that this compound is effective in mimicking the plectin knock-out phenotype, including responsiveness.[5] Additionally, the mitochondrial chaperone HSP60 (also known as HSPD1) was identified as a target for a porphyrin-based gold(III) complex *via* photoaffinity labelling[6] and a cyclometalated gold(III) compound was shown to target multiple proteins.[7] An arsenic-based probe was recently developed to characterize the target landscape of arsenic trioxide in cancer cells, and HSP60 was also found among the direct interactors.[8]

Together with other omics technologies,[9] target identification methods underscored the original promise that this

[*] Dr. B. Neuditschko,[+] L. Janker, Dr. A. Bileck, Y. Borutzki, Prof. C. Gerner, Prof. S. M. Meier-Menches
Department of Analytical Chemistry, Faculty of Chemistry, University of Vienna
1090 Vienna (Austria)
E-mail: samuel.meier-menches@univie.ac.at

Dr. B. Neuditschko,[+] Y. Borutzki, Prof. S. M. Meier-Menches
Institute of Inorganic Chemistry, Faculty of Chemistry, University of Vienna
1090 Vienna (Austria)

Dr. A. P. King,[+] Z. Huang, Dr. S. C. Marker, Prof. J. J. Wilson
Department of Chemistry and Chemical Biology, Cornell University
Ithaca, NY 14853 (USA)
E-mail: jjw275@cornell.edu

L. Janker, Dr. A. Bileck, Prof. C. Gerner, Prof. S. M. Meier-Menches
Joint Metabolome Facility, University of Vienna and Medical University Vienna
1090 Vienna (Austria)

Dr. B. Neuditschko[+]
Present address: Institute Krems Bioanalytics, IMC University of Applied Sciences Krems
3500 Krems (Austria)

Dr. A. P. King,[+] Dr. S. C. Marker
Present address: Chemical Biology Laboratory, Center for Cancer Research, National Cancer Institute
Frederick, MD 21702 (USA)

[+] These authors contributed equally to this work.

class of metal-based therapeutics modulates novel targets and often by unprecedented modes of action.[2b,10] Therefore, it is of current interest to expand the insight into metallodrug target interactions and landscapes. It is also often not entirely understood how molecular reactivities and ligand exchange reactions are translated into biological effects,[3a] although it is known that small structural changes of the metallodrug can considerably modify the potential target landscape.[4a]

The target landscapes of the family of rhenium compounds is largely underexplored with one notable exception,[11] despite the fact that rhenium carbonyls are actively investigated with respect to their medicinal applications in diagnosis and therapy.[12] For example, a rhenium tricarbonyl inhibited the phosphorylation of aurora kinase A and thus led to a G2/M cell cycle arrest.[13]

Recently, some of us discovered that $[Re(CO)_3(dmphen)(p\text{-tol-ICN})]^+$ (TRIP), where dmphen = 2,9-dimethyl-1,10-phenanthroline and *p*-tol-ICN = *para*-tolyl isonitrile, is an active anticancer agent *in vivo* (Scheme 1A).[14] TRIP is a rhenium tricarbonyl compound that contains a stable axial isonitrile ligand, and which accumulates mainly in the cytosol.[15] Mechanistic investigations concluded that TRIP leads to fast protein aggregation, which induces endoplasmic reticulum (ER) stress, over-activates the unfolded protein response (UPR) pathways and subsequently triggers apoptosis.[15b] TRIP showed no involvement of the proteasome, heat shock protein 90 (HSP90) or reactive oxygen species (ROS) in its mode of action.[15b] In TRIP-resistant ovarian cancer cells upregulated multidrug resistance transporter 1 and metallothionein 1E suggested increased efflux and metal detoxification as probable resistance mechanisms.[16]

Here, we describe the synthesis of a biotin-labelled TRIP analogue together with the characterization of its target landscape by chemical proteomics in the ovarian cancer cell line A2780 in a dose-dependent manner to prioritize potential drug targets.[17] Moreover, we characterize the cellular response to TRIP-treatment by proteome profiling in the same cell line using a label free quantification (LFQ) approach.[18] Together, these data revealed the Fe–S cluster assembly factor NUBP2 (NUBP2, Q9Y5Y2) as a potential target protein of TRIP, which was competitively saturated by 100 nM free TRIP. Accordingly, we found a down-regulation of Fe–S cluster containing proteins and upregulated ferritin in treated cells. A disturbance of Fe–S cluster-containing proteins in cellular respiration was further verified by assessing mitochondrial bioenergetics. Thus, NUBP2 represents a promising target of TRIP at subcytotoxic concentrations.

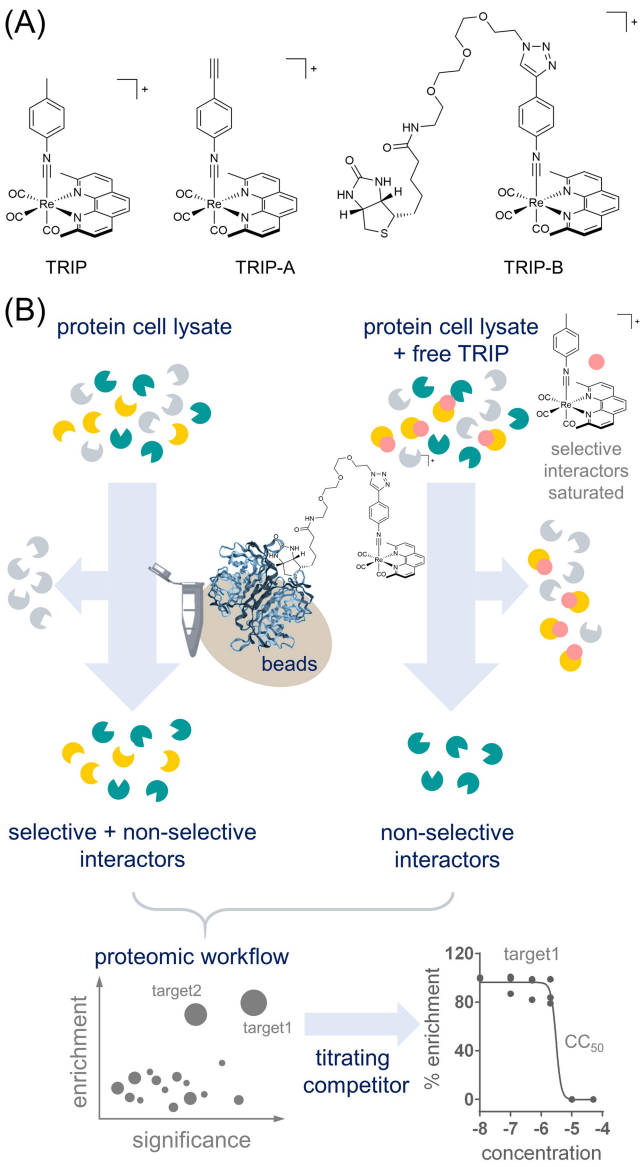

Scheme 1. A) Molecular structures of the rhenium tricarbonyls investigated in this study. B) Workflow of the chemical proteomics approach to profile drug-protein interactions. In a competition binding assay, affinity purifications with free TRIP saturate the selective interactors so that only nonselective interactors remain. Those can be subtracted from the normal pull-down to obtain selective interactors. Increasing concentrations of the free competitor lead to depletion of a potential target. The potency of interaction can be characterized by the concentration at which half of the target protein was competitively saturated by free TRIP (CC_{50}).

Results and Discussion

A biotin-labelled TRIP (TRIP-B) was synthesized in order to determine the target landscape of TRIP by chemical proteomics (Scheme 1A). This approach was previously shown to be highly effective in enriching also low abundant protein targets from whole cell lysates.[4b] TRIP was labelled at the stable isonitrile ligand[15a] to reduce the likelihood of ligand cleavage from the metal center. Moreover, biotin and TRIP are connected by a hydrophilic PEG linker, which ensures a low tendency for nonspecific hydrophobic interactions during the affinity purification step. TRIP is generally inert and expected to interact with potential protein targets primarily through noncovalent bonds. TRIP-B was accessed *via* an alkyne-modified isonitrile ligand (TRIP-A, Scheme 1A). The axial isonitrile ligand of TRIP-

A was prepared using the Hoffmann carbylamine reaction beginning with *p*-alkynyl aniline. This isonitrile was then attached to *fac*-Re(dmphen)$(CO)_3$OTf using previously reported methods.[14]

An alkyne handle was chosen for TRIP-A due to the modular accessibility of novel TRIP conjugates using click chemistry. The resultant alkyne-tagged TRIP-A complex was conjugated to biotin-PEG-N_3 through the well-established copper-catalyzed azide-alkyne cycloaddition (CuAAC) reaction. TRIP-A was found to be very amenable to the CuAAC reaction, for incubating TRIP-A and biotin-PEG-N_3 in acetonitrile containing cupric sulfate, tris(benzyltriazolylmethyl)amine, and ascorbic acid overnight afforded quantitative generation of TRIP-B. Separation of the conjugate from the starting reagents by preparatory HPLC afforded the product in high yield. The purity and identity of TRIP-B were verified by HPLC, ^{1}H NMR, and ESI-HRMS (Supporting Information Figures 1–4). The effective concentration of TRIP to inhibit 50 % cell growth (EC_{50}) in the ovarian cancer cell line A2780 after 24 h treatment was found to be 1.4 ± 0.6 μM. This value matches previous reports (Supporting Information Figure 5).[15b]

Target Landscape of TRIP

Chemoproteomic profiling was performed using a biotin-streptavidin immobilization strategy. The biotin-labelled TRIP-B (200 nmol) was incubated with half-equivalents of streptavidin binding sites on beads (100 nmol) for 30 min. Native cell lysates of the ovarian cancer cell line A2780 were prepared for this study as TRIP was previously studied in this cell line.[15b,16] The equivalent of around 10^7 cells from an 80 % confluent T75 cell culture flask was used for preparing the cell lysate of one replicate. In order to prioritize selective interactors of TRIP, we performed a competitive pull-down with TRIP in a dose-dependent manner.[17] Besides the normal pull-down, where the cell lysates were directly mixed with the immobilized TRIP-B, we also performed competitive pull-downs, where the free TRIP was exposed to the cell lysate prior to the interaction with the immobilized TRIP-B on the beads (Scheme 1B). This pretreatment occupies selective binding sites and only non-selective binding sites remain. By subtracting the competitive from the normal pull-down, it is possible to visualize the selective interactors according to their pull-down enrichment. Moreover, we performed the competition experiments at increasing TRIP concentrations corresponding to 0.1, 0.5, 2, 10 and 50 μM (1 mL, T75 equivalents) in order to observe dose-dependent saturation curves. This implies that with increasing concentration of the free competitor, the binding sites will be saturated and the protein interactor will disappear in a dose-dependent manner in the proteomic experiment. Each condition was carried out in triplicates amounting to three normal and 15 competitive pull-downs. The affinity-purified proteins were directly digested on the beads by trypsin/Lys-C and subsequently analyzed by mass spectrometry based LFQ proteomics.[19]

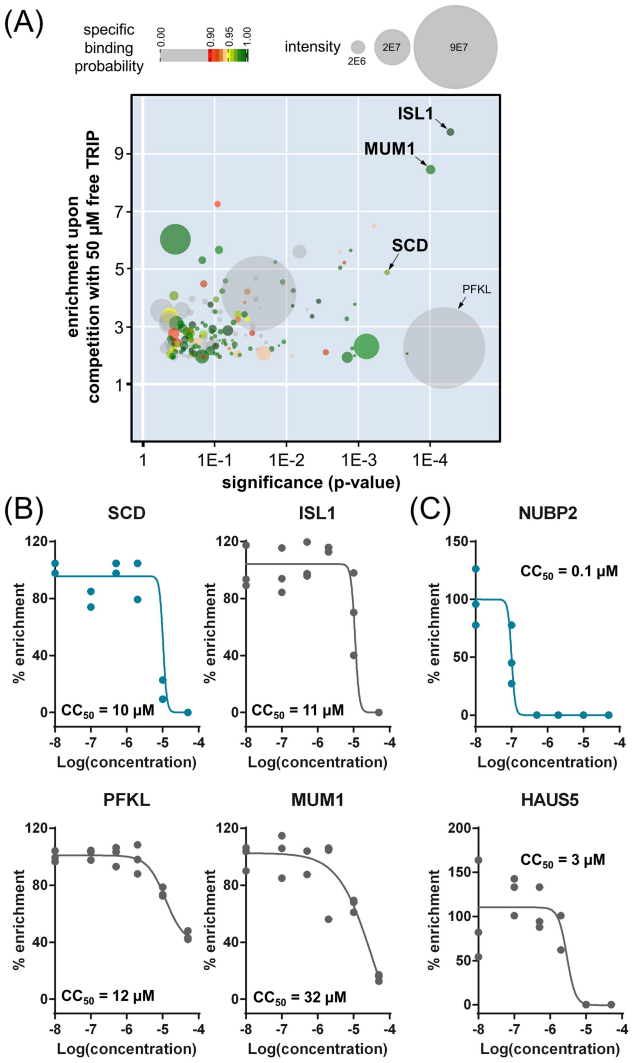

Figure 1. A) Result of the chemoproteomic approach using 50 μM of free TRIP as competitor. A total of 2513 proteins were identified in the pull-downs. The 171 proteins with at least 2-fold enrichment are shown. ISL1 = Insulin gene enhancer protein ISL-1 (P61371), MUM1 = PWWP domain containing protein MUM1 (Q2TAK8), SCD = Acyl-CoA desaturase (O00767), and PFKL = ATP-dependent 6-phosphofructokinase (P17858). B) The inhibition profiles of the indicated potential interactors are shown and their concentrations at which half of the target protein was competitively saturated by free TRIP (CC_{50}) are highlighted. This competition value was obtained from a sigmoidal fit of LFQ values and serves as a measure of potency. C) Exemplary saturation profiles of two potent interactors for free TRIP are shown. NUBP2 = Cytosolic Fe–S cluster assembly factor NUBP2 (Q9Y5Y2), HAUS5 = HAUS augmin-like complex subunit 5 (O94927).

A total of 2513 protein groups were identified in the entire chemoproteomic approach. Filtering conditions included finding a given protein in three out of three replicates in at least one condition. Furthermore, match between runs was disabled during the MaxQuant search.[20] Of these, 736 proteins were found with ≥3 unique peptides. Free TRIP competitively saturated several potential interactors in a dose-dependent manner. Their number increased with the concentration of the competitor: 10 proteins at 0.1 μM, 15

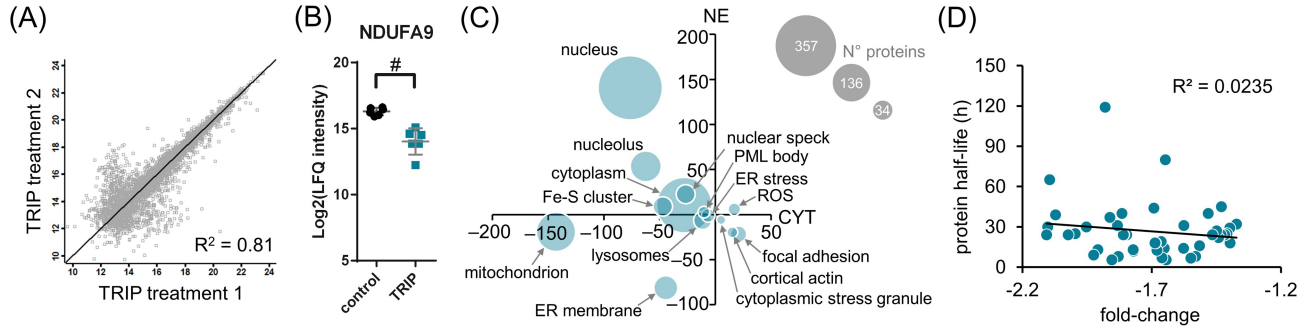

Figure 2. A) Proteomic response profiling of TRIP-treated A2780 cancer cells identified 5457 protein groups in total (grey squares). The scatter plot reveals the intensity correlation of two independent biological replicates. B) Proteomic response profiling was carried out in hexuplicates. The chart shows the multi-parameter corrected significant (#) protein regulation of NDUFA9, a component of the mitochondrial respiratory complex I. C) The significantly regulated proteins were grouped according to cellular compartment and functional groups and displayed as the regulome upon TRIP treatment. The *x*- and *y*-axes show the summed protein regulation in the cytoplasmic (CYT) and nuclear (NE) fraction, respectively. The size of the bubble corresponds to the number of proteins in the group. D) The down-regulated cytoplasmic proteins did not reveal a correlation of protein half-lives with fold change.

proteins at 0.5 μM, 16 proteins at 2 μM, 43 proteins at 10 μM and 41 proteins at 50 μM competitor concentration, yielding a total of 89 interactors (Supporting Information Figure 6 and Supporting Information Table 1). The proteins with potent competition at low dose are deemed most relevant to the mode of action of TRIP. These proteins did not reveal enriched GO terms, nor network interactions, which underlines that these probable targets do not stem from intact protein complexes and constitute unique hits. The large number of proteins detected in the pull-down may also reflect the proteotoxic properties of TRIP at higher doses. Here, we are especially interested in the specific effects at sub-cytotoxic doses. Furthermore, the proteins neither feature significantly enriched consensual sequences, suggesting that TRIP is not selectively targeting a particular consensual sequence. The most enriched sequence was a tetratricopeptide-like helical domain (6 proteins, 7 %, Benjamini-corrected p-value = 0.83), which controls protein-protein interactions.[21]

The competition experiment using 50 μM competitor returned 171 potential interactors with an enrichment factor of ≥ 2 (Figure 1A). Among the most significantly enriched proteins, we identified insulin gene enhancer protein ISL-1 (ISL1, P61371), PWWP domain containing protein MUM1 (MUM1, Q2TAK8), Acyl-CoA desaturase (SCD, O00767) and ATP-dependent 6-phosphofructokinase (PFKL, P17858). The latter was found with high intensity, but corresponds to a low-specific interactor as calculated by means of the CRAPome database.[22] Nonetheless, these four interactors displayed a dose-dependent competition profile with concentrations at which half of the target protein was competitively saturated by free TRIP (CC_{50}) between 10–32 μM (Figure 1B). SCD was the most potent interactor at this dose level showing a $CC_{50} = 10$ μM. The nonspecific PFKL did not show complete saturation. Finally, cytosolic Fe–S cluster assembly factor NUBP2 (NUBP2, Q9Y5Y2) and HAUS augmin-like complex subunit 5 (HAUS5, O94927) were among the most potent interactors overall featuring CC_{50} values of 0.1 μM and 3 μM, respectively (Figure 1C).

During the course of the preparation of this manuscript, Yim and Park published a label-free target identification approach with TRIP based on thermal denaturation.[11] They reported and validated HSP60 as a target interactor for TRIP in HeLa cancer cells and determined a dissociation constant of approximately 2 μM. Here, we detected HSP60 (HSPD1, P10809) in the chemoproteomic data set, but it was not competitively saturated by free TRIP in a dose-dependent manner (Supporting Information Figure 7A). However, the CC_{50} values for potential interactors in our study were in a similar range, covering 0.1–32 μM.

Proteomic Response to TRIP Treatment

Because we used a chemoproteomic approach with cell lysates, we also set out to characterize the proteomic response of living A2780 cancer cells to the treatment of sub-cytotoxic concentrations of TRIP. For this purpose, cells were treated at half-IC_{50} concentration for 24 h in hexuplicates. The samples were digested with trypsin/Lys-C and each peptide fraction was analyzed by an LFQ proteomics approach[18] using a timsTOF Pro mass spectrometer,[19] in a similar manner compared to the target profiling experiments. A total of 5457 protein groups were identified. Multiparameter-corrected significant regulations of protein abundance were calculated by FDR = 0.05 and S0 = 0.1. The nucleocytoplasmic fractionation revealed 380 significant protein regulations in the cytoplasmic and 420 significant protein regulations in the nuclear fraction. From unimputed data, the R^2 of biological replicates of treated samples was typically around 0.8 (Figure 2A).

When considering subcellular fractions and the direction of regulation, it was revealed that mainly the 237 significantly down-regulated cytoplasmic proteins featured enriched gene ontology (GO) term sets. GO terms categorize genes according biological processes, molecular functions,

cellular compartments or pathways and enable extracting functional or pathway information of interventions. They correspond to mitochondrial translational elongation (23 counts, Benjamini-corrected p-value $= 1{,}8 \times 10^{-20}$), mitochondrial respiratory chain complex I (19 counts, Benjamini-corrected p-value $= 5{,}7 \times 10^{-17}$), DNA repair (14 counts, Benjamini-corrected p-value $= 4{,}5 \times 10^{-3}$), and cholesterol biosynthetic process (6 counts, Benjamini-corrected p-value $= 1{,}1 \times 10^{-2}$). The down-regulated complex I protein NDUFA9 exemplifies the variance of the experimental setup (Figure 2B).

In order to obtain a global overview of the proteomic response of the A2780 cancer cells to the TRIP treatment, the 774 significantly regulated proteins were bundled into 14 groups according to their cellular compartments, as well as functions. The cytoplasmic and nuclear protein fold changes were then summed up and displayed in a 2D plot, showing the protein regulations in the cytoplasmic and the nuclear fractions on the *x*- and *y*-axes, respectively (Figure 2C). The size of the bubbles represents the number of proteins included in each group. This visualization of the global protein regulations is termed the regulome, in analogy to the transcriptomic term regulon.[23]

The lack of protein groups in the quadrant of upregulated cytoplasmic and nuclear proteins is a striking feature in comparison to previous regulomes obtained with other metal-based anticancer drug candidates containing gold or ruthenium.[4a,18] This result might reflect the ability of TRIP to lead to translation inhibition in A2780 cancer cells. However, cytoplasmic ribosomal proteins were not regulated, while 23 mitochondrial ribosomal proteins were down-regulated in the cytoplasmic fraction. They are included in the *mitochondrion* group in Figure 2C and highlighted in Supporting Information Figure 7B. Translation inhibition would also be represented by a down-regulation of proteins with short half-lives in cells.[24] We therefore plotted 51 down-regulated cytoplasmic proteins according to their protein half-lives and fold changes (Figure 2D). There was no observable correlation between the two variables. Thus, translation inhibition cannot be conclusively inferred from the sub-cytotoxic treatment of A2780 cancer cells with TRIP. Moreover, the regulome also featured a lack of heat shock proteins and proteasomal components, which matches previous findings with TRIP.[15b] Previous reports also indicate a lack of ROS induction upon treating A2780 cancer cells with TRIP. Interestingly, the ROS-associated protein group was the single group to be upregulated in both cytoplasmic and nuclear fractions (Figure 2C). The 16 proteins are represented by ROS-managing enzymes, e.g. HMOX1 (P09601), NQO1 (P15559), FECH (P22830), GPX4 (P36969), ME1 (P48163) and TXNRD2 (Q9NNW7), and their considerable upregulation might explain the lack of ROS formation. Finally, the known effect of TRIP on the UPR of the endoplasmic reticulum (ER) was evidenced by reduced ER membrane components and slightly upregulated ER stress-associated proteins. The latter contains protein Niban (FAM129 A, Q9BZQ8), which regulates the activity of eIF2α, to influence protein translation and may be a late player in the ER stress response.[25]

With the exception of translation inhibition, the proteome profiling carried out in this study confirmed the main findings of the mode of action of TRIP. The lack of markers for translation inhibition may be due to the sub-cytotoxic treatment concentration (half-IC_{50}).

TRIP Targets Are Prioritized by Target-Response Networks

A drawback of the chemoproteomic approach is that the experiment is performed using cell lysates, which might not necessarily reflect the conditions in living cells and not account for drug distribution. Nonetheless, probable targets can be prioritized by either dose-dependent competition[17] or target-response networks.[4b] For TRIP, we combined both of these approaches.

Target-response networks are built on the assumption that a true target interaction between a drug and a protein in a cell will lead to perturbations in the protein network around this target, which should be detectable by proteomic profiling of drug-treated cells. It can be expected that highly probable targets will be extensively connected to perturbed proteins in these networks. In contrast, biologically non-relevant protein targets will be characterized by the absence of protein perturbations around the target. Out of the probable targets revealed by dose-dependent competition curves only NUBP2 and SCD generated relevant target-response networks ranking these proteins as top candidates for further validation (Figure 3). Acyl-CoA desaturase (SCD) showed a $CC_{50} = 10\ \mu M$ in the dose-dependent chemoproteomic profiling. This concentration suggested that SCD is hardly inhibited at pharmacologically relevant doses of TRIP. Despite that SCD is an interesting anticancer target in metabolically compromised environments because it is important in the formation of unsaturated fatty acids and thus, membrane integrity and other lipid functions.[26]

Being a fatty acid desaturase, SCD introduces the first double bond into saturated fatty acyl-coenzyme A substrates.[27] As such, SCD is found to be tightly connected to lipid and sterol biosynthesis in the target-response network (Figure 3A). Interestingly, these proteins were all down-regulated upon treatment with TRIP. For example, fatty acid desaturases 1 (FADS1, O60427) and 2 (FADS2, O95864) are involved in lipogenesis, while proteins of sterol biosynthesis include CYP51A1 (Q16850), MSMO1 (Q15800), DHCR24 (Q15392), and HMGCS1 (Q01581). Several of these proteins were also present in the ER membrane and/or ER stress groups in the regulome (Figure 2C). The down-regulation of these lipid-associated proteins may disturb the energy and redox balance in cells and lead to the upregulation of redox proteins that manage oxidative stress. Indeed, the Nrf2 target genes HMOX1 (P09601) and NQO1 (P15559) were found to be upregulated. Lipid biosynthesis critically contributes to the anabolism of membrane building blocks, which are required for proper ER function even when proteostasis is intact.[28] Consequently, the target-response network suggests that SCD might constitute a probable target for TRIP. To test the inhibitory property of TRIP on SCD, we performed

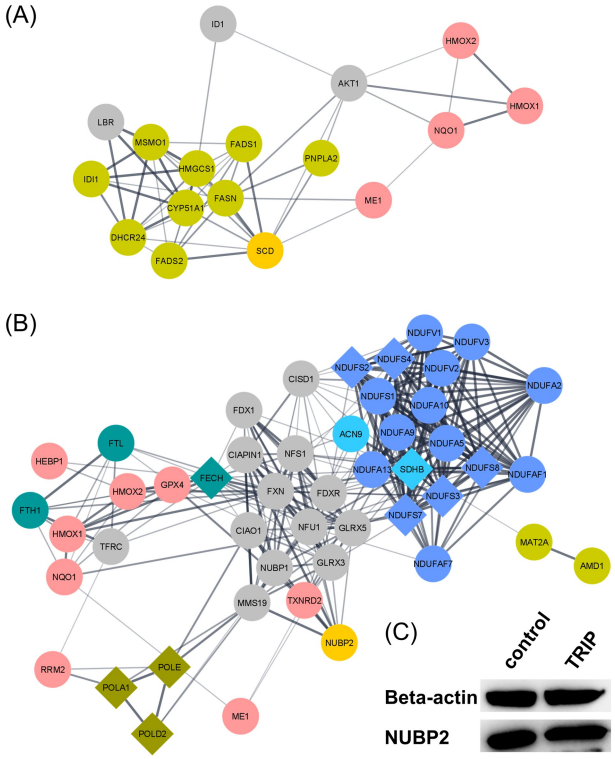

Figure 3. Target-response networks connect potential targets of TRIP obtained from the chemoproteomic approach to TRIP-induced proteome changes in A2780 cancer cells. A) Target-response network for Acyl-CoA desaturase (SCD, O00767). SCD (orange) directly modulates lipid and sterol-associated proteins (green) and also connects to redox regulating proteins (rose). B) Target-response network of cytosolic Fe–S cluster assembly factor NUBP2 (NUBP2, Q9Y5Y2). NUBP2 (orange) is part of the Fe–S cluster biogenesis (grey, not regulated), which connects to Fe–S containing proteins of DNA repair (POLD2, dark yellow), as well as mitochondrial complex I NADH dehydrogenase (dark blue), complex II succinate dehydrogenase (light blue), and *S*-adenosylmethionine-associated proteins (MAT2 A and AMD1, yellow). Fe–S biogenesis is also associated with redox proteins (rose) and iron storage (turquois). Fe–S cluster containing proteins are shown in a diamond shape. C) Western blot analysis of NUBP2 expression in control and TRIP-treated cells, normalized to protein content.

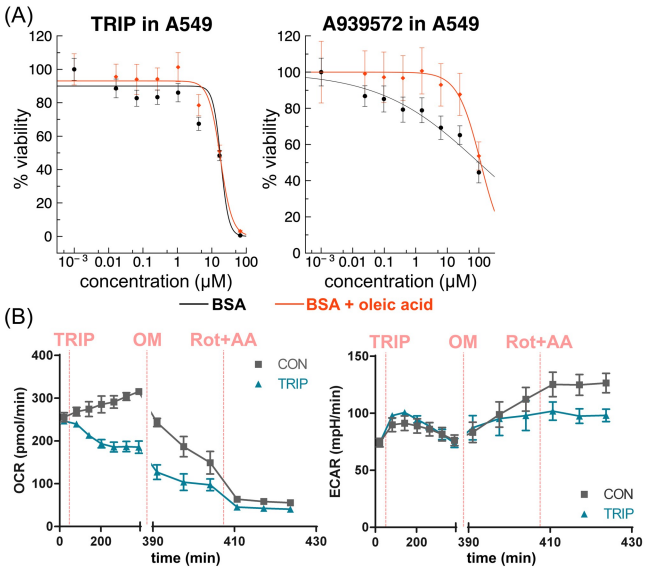

Figure 4. A) Viability assays with TRIP were carried out in presence of bovine serum albumin (BSA) or BSA loaded with oleic acid (30 μM) in A549 lung cancer cells. The SCD inhibitor A939572 served as a positive control. B) Oxygen consumption rate (OCR) and extracellular acidification rate (ECAR) of mock-treated (grey) and TRIP-treated A2780 cancer cells (IC_{50}, 6 h, blue). Oligomycin (OM) inhibits ATP synthase, while Rotenone (Rot) and Antimycin-A (AA) block respiratory complex I and III, respectively.

cytotoxicity assays in the absence and presence of oleic acid (30 μM), an 18:1 fatty acid that is among the products of SCD activity. Inhibition of SCD will deplete the pool of unsaturated fatty acids in cells, which can be rescued by the supplementation with oleic acid. Thus, supplementation with oleic acid is expected to reduce the potency of TRIP in the viability assay if SCD would be a true target,[29] but we observed no such effect in A549 cancer cells (Figure 4A), nor in A2780 cancer cells (Supporting Information Figure 9). In contrast, the SCD inhibitor A939572 showed a clear rescuing effect by oleic acid (Figure 4A). This result suggests that SCD is not a target of TRIP at pharmacologically relevant concentrations and confirms that the unfolded protein response in the ER is indeed caused by proteotoxic rather than lipotoxic effects.

In contrast, the Fe–S cluster assembly factor NUBP2 showed the most potent CC_{50} of 0.1 μM out of the entire series of potential targets. NUBP2 deficiency in humans is not reported, but the ortholog Nbp35 seems to be essential in yeast.[30] NUBP2 is part of the Fe–S cluster biogenesis machinery,[31] of which several components were detected, including NUBP1 (P53384), GLRX3 (O76003), GLRX5 (Q86SX6), FDXR (P22570), FXN (Q16595), FDX1 (P10109), NFU1 (Q9UMS0), NFS1 (Q9Y697) and CIAO1 (O76071, all grey, Figure 3B and Supporting Information Figure 8A).[30,32] These proteins were not regulated upon treatment with TRIP. In mammals, Fe–S clusters are typically found in complex I and complex II of oxidative phosphorylation, aconitase,[30] as well as DNA repair proteins[33] and depend on iron availability. Down-regulation of complex I proteins was among the most significant changes in the overall GO term analysis. Interestingly, we found many known Fe–S cluster containing proteins in the target-response network (Figure 3B, highlighted in diamond shape). NADH dehydrogenase iron-sulfur proteins (NDUFS2-4 and NDUFS8, O00217), succinate dehydrogenase iron-sulfur subunit (SDHB, P21912) and the DNA polymerases alpha (POLA1, P09884) and epsilon (POLE, Q07864) were all down-regulated by TRIP, as also indicated in the regulome (Figure 2C), while ferrochelatase (FECH, P22830) and DNA polymerase D2 (POLD2, P49005) were slightly upregulated (Supporting Information Figure 8B). Interestingly, the iron storage proteins ferritin light chain (FTL, P02792), heavy chain (FTH1, P02794), as well as arylsulfatase A (ARSA, P15289) were upregulated indicating a feedback effect of Fe–S cluster depletion (Supporting Information Figure 8C). Concomitantly, ROS managing

proteins were also upregulated (see above). Of note, the protein expression of NUBP2 is not altered upon treatment with TRIP as determined by western blot (Figure 3C). The combination of potent CC_{50} in the dose-dependent pull-down and the details of the target-response network strongly suggest NUBP2 to be a potential high affinity target of TRIP. Interestingly, the scaffold protein NUPB2 was not yet reported as a drug target to the best of our knowledge, while targeting Fe–S cluster biogenesis was suggested to be a promising anticancer strategy because of the addiction of some cancer types to iron.[34] The down-regulation of key Fe–S cluster containing proteins as a direct consequence of targeting the scaffold protein NUBP2 is a striking feature of the mode of action of TRIP at sub-cytotoxic concentrations.

Mitochondrial bioenergetics crucially depends on the presence of Fe–S clusters in complexes I and II of cellular respiration. To this end, we verified the downstream effect of TRIP on Fe–S cluster biogenesis using a Seahorse assay test kit by assessing the cellular oxygen consumption rate (OCR) and the extracellular acidification rate (ECAR). A2780 cells were treated with TRIP (IC_{50}, 6 h) and constantly monitored over this time period (Figure 4B). Then, cellular respiration was successively inhibited with Oligomycin (OM, complex V) and Rotenone-Antimycin A (Rot + AA, complexes I and III). The treatment with TRIP led to an immediate decrease in the OCR, which stabilized after 3–4 h. Inhibition of complex V had a differential effect on control (grey) and TRIP-treated (blue) cells indicating that the capacity of Fe–S containing protein complexes I and II is reduced and that the OCR reduction may be roughly proportional to the turnover of key complex I proteins.[24] The complete inhibition of cellular respiration by Rot + AA led to similar OC rates on control and treated cells suggesting that the major effect of the observed difference was indeed due to complexes I and II. In contrast, the ECAR differed only upon complete inhibition of cellular respiration, where the treatment resulted in a reduced ECAR suggesting additional effects at play that potentially relate to the broad proteotoxic effect of TRIP (Figure 4B).

In summary, combining dose-dependent chemoproteomics with target-response networks allowed the successful identification of prioritized protein targets for the rhenium drug candidate TRIP. We identified the scaffold protein Fe–S cluster biogenesis factor NUBP2 as a competitively saturated target of TRIP at nanomolar concentrations. Treated cancer cells displayed down-regulated Fe–S cluster containing proteins and upregulated ferritin. Targeting Fe–S cluster biogenesis was further verified by assessing mitochondrial oxygen consumption rates and suggest that besides its broad proteotoxic effects, TRIP may selectively disrupt Fe–S cluster biogenesis at sub-cytotoxic concentrations.

Author Contributions

PK and SCM synthesized compounds, BN, ZH and SMM performed cell culture experiments, ZH performed western blotting, BN and SMM performed pull-downs and sample preparation, LJ and AB carried out LC-MS/MS and bioinformatic analyses, YB performed the Seahorse experiments, SMM and CG evaluated the data, SMM and JW wrote the initial draft of the manuscript, which was approved by all authors.

Acknowledgements

BN, LJ, AB, CG and SMM are grateful to the Core Facility for Mass Spectrometry (Faculty of Chemistry, University of Vienna) and the Joint Metabolome Facility (University of Vienna and Medical University Vienna), which are both members of the Vienna Life-Science Instruments (VLSI). B.N. is funded by the GFF-NÖ (Stiftungsprofessur 'Clinical Proteomics') Krems.

Conflict of Interest

The authors declare no conflict of interest.

Data Availability Statement

The data that support the findings of this study are openly available in PRIDE at http://proteomecentral.proteomexchange.org/cgi/GetDataset, reference number 34466.

Keywords: Cancer · Mode of Action · Proteomics · Rhenium · Target Identification

[1] K. Kubota, M. Funabashi, Y. Ogura, *Biochim. Biophys. Acta Proteins Proteomics* **2019**, *1867*, 22–27.
[2] a) J. Ha, H. Park, J. Park, S. B. Park, *Cell Chem. Biol.* **2021**, *28*, 394–423; b) Y. Wang, H. Li, H. Sun, *Inorg. Chem.* **2019**, *58*, 13673–13685.
[3] a) D. Kreutz, C. Gerner, S. M. Meier-Menches, in: *Metal-based anticancer agents* (Eds.: A. Casini, A. Vessieres, S. M. Meier-Menches), Royal Society of Chemistry, London, **2019**, pp. 246–270; b) M. Bantscheff, S. Lemeer, M. M. Savitski, B. Kuster, *Anal. Bioanal. Chem.* **2012**, *404*, 939–965.
[4] a) S. M. Meier-Menches, K. Zappe, A. Bileck, D. Kreutz, A. Tahir, M. Cichna-Markl, C. Gerner, *Metallomics* **2019**, *11*, 118–127; b) S. M. Meier, D. Kreutz, L. Winter, M. H. M. Klose, K. Cseh, T. Weiss, A. Bileck, B. Alte, J. C. Mader, S. Jana, et al., *Angew. Chem. Int. Ed.* **2017**, *56*, 8267–8271; *Angew. Chem.* **2017**, *129*, 8379–8383.
[5] M. Prechova, Z. Adamova, A.-L. Schweizer, M. Maninova, A. Bauer, D. Kah, S. M. Meier-Menches, G. Wiche, B. Fabry, M. Gregor, *J. Cell Biol.* **2022**, *221*, e202105146.
[6] D. Hu, Y. Liu, Y.-T. Lai, K.-C. Tong, Y.-M. Fung, C.-N. Lok, C.-M. Che, *Angew. Chem. Int. Ed.* **2016**, *55*, 1387–1391; *Angew. Chem.* **2016**, *128*, 1409–1413.
[7] S. K. Fung, T. Zou, B. Cao, P.-Y. Lee, Y. M. E. Fung, D. Hu, C.-N. Lok, C.-M. Che, *Angew. Chem. Int. Ed.* **2017**, *56*, 3892–3896; *Angew. Chem.* **2017**, *129*, 3950–3954.
[8] X. Hu, H. Li, T. K.-Y. Ip, Y. F. Cheung, M. Koohi-Moghadam, H. Wang, X. Yang, D. N. Tritton, Y. Wang, Y. Wang, et al., *Chem. Sci.* **2021**, *12*, 10893–10900.

[9] a) H. Wang, Y. Zhou, X. Xu, H. Li, H. Sun, *Curr. Opin. Chem. Biol.* **2020**, *55*, 171–179; b) I. Romero-Canelón, P. J. Sadler, *Proc. Natl. Acad. Sci. USA* **2015**, *112*, 4187–4188.
[10] S. M. Meier-Menches, C. Gerner, W. Berger, C. G. Hartinger, B. K. Keppler, *Chem. Soc. Rev.* **2018**, *47*, 909–928.
[11] J. Yim, S. B. Park, *Front. Chem.* **2022**, *10*, 850638.
[12] a) K. Schindler, F. Zobi, *Molecules* **2022**, *27*, 539; b) Z. Huang, J. J. Wilson, *Eur. J. Inorg. Chem.* **2021**, 1312–1324; c) A. Domenichini, I. Casari, P. V. Simpson, N. M. Desai, L. Chen, C. Dustin, J. S. Edmands, A. van der Vliet, M. Mohammadi, M. Massi, et al., *J. Exp. Clin. Cancer Res.* **2020**, *39*, 276; d) C. C. Konkankit, B. A. Vaughn, Z. Huang, E. Boros, J. J. Wilson, *Dalton Trans.* **2020**, *49*, 16062–16066; e) Z.-Y. Pan, D.-H. Cai, L. He, *Dalton Trans.* **2020**, *49*, 11583–11590.
[13] P. V. Simpson, I. Casari, S. Paternoster, B. W. Skelton, M. Falasca, M. Massi, *Chem. Eur. J.* **2017**, *23*, 6518–6521.
[14] S. C. Marker, A. P. King, S. Granja, B. Vaughn, J. J. Woods, E. Boros, J. J. Wilson, *Inorg. Chem.* **2020**, *59*, 10285–10303.
[15] a) C. C. Konkankit, J. Lovett, H. H. Harris, J. J. Wilson, *Chem. Commun.* **2020**, *56*, 6515–6518; b) A. P. King, S. C. Marker, R. V. Swanda, J. J. Woods, S. B. Qian, J. J. Wilson, *Chem. Eur. J.* **2019**, *25*, 9206–9210.
[16] S. C. Marker, A. P. King, R. V. Swanda, B. Vaughn, E. Boros, S. B. Qian, J. J. Wilson, *Angew. Chem. Int. Ed.* **2020**, *59*, 13391–13400; *Angew. Chem.* **2020**, *132*, 13493–13502.
[17] S. Klaeger, S. Heinzlmeir, M. Wilhelm, H. Polzer, B. Vick, P.-A. Koenig, M. Reinecke, B. Ruprecht, S. Petzoldt, C. Meng, et al., *Science* **2017**, *358*, eaan4368.
[18] S. M. Meier-Menches, B. Neuditschko, K. Zappe, M. Schaier, M. C. Gerner, K. G. Schmetterer, G. Del Favero, R. Bonsignore, M. Cichna-Markl, G. Koellensperger, et al., *Chem. Eur. J.* **2020**, *26*, 15528–15537.
[19] A. Bileck, P. Bortel, M. Kriz, L. Janker, E. Kiss, C. Gerner, G. Del Favero, *Front. Oncol.* **2022**, *11*, 746411.
[20] S. Tyanova, T. Temu, J. Cox, *Nat. Protoc.* **2016**, *11*, 2301–2319.
[21] L. D. D′Andrea, L. Regan, *Trends Biochem. Sci.* **2003**, *28*, 655–662.
[22] D. Mellacheruvu, Z. Wright, A. L. Couzens, J.-P. Lambert, N. A. St-Denis, T. Li, Y. V. Miteva, S. Hauri, M. E. Sardiu, T. Y. Low, et al., *Nat. Methods* **2013**, *10*, 730–736.
[23] S. Reich, C. D. L. Nguyen, C. Has, S. Steltgens, H. Soni, C. Coman, M. Freyberg, A. Bichler, N. Seifert, D. Conrad, et al., *Nat. Commun.* **2020**, *11*, 2936.
[24] J. Zecha, C. Meng, D. P. Zolg, P. Samaras, M. Wilhelm, B. Kuster, *Mol. Cell. Proteomics* **2018**, *17*, 974–992.
[25] G. D. Sun, T. Kobayashi, M. Abe, N. Tada, H. Adachi, A. Shiota, Y. Totsuka, O. Hino, *Biochim. Biophys. Acta Proteins Proteomics* **2007**, *360*, 181–187.
[26] B. Peck, Z. T. Schug, Q. Zhang, B. Dankworth, D. T. Jones, E. Smethurst, R. Patel, S. Mason, M. Jiang, R. Saunders, et al., *Cancer Metab.* **2016**, *4*, 6.
[27] M. T. Flowers, J. M. Ntambi, *Curr. Opin. Lipidol.* **2008**, *19*, 248–256.
[28] a) N. S. Hou, A. Gutschmidt, D. Y. Choi, K. Pather, X. Shi, J. L. Watts, T. Hoppe, S. Taubert, *Proc. Natl. Acad. Sci. USA* **2014**, *111*, E2271–E2280; b) J. Han, R. J. Kaufman, *J. Lipid Res.* **2016**, *57*, 1329–1338.
[29] U. V. Roongta, J. G. Pabalan, X. Wang, R.-P. Ryseck, J. Fargnoli, B. J. Henley, W.-P. Yang, J. Zhu, M. T. Madireddi, R. M. Lawrence, et al., *Mol. Cancer Res.* **2011**, *9*, 1551–1561.
[30] N. Maio, T. A. Rouault, *Trends Biochem. Sci.* **2020**, *45*, 411–426.
[31] X. Fan, W. D. Barshop, A. A. Vashisht, V. Pandey, S. Leal, S. Rayatpisheh, Y. Jami-Alahmadi, J. Sha, J. A. Wohlschlegel, *J. Biol. Chem.* **2022**, *298*, 102094.
[32] N. Maio, T. A. Rouault, *Biochim. Biophys. Acta Mol. Cell Res.* **2015**, *1853*, 1493–1512.
[33] a) R. Shi, W. Hou, Z.-Q. Wang, X. Xu, *Front. Cell Dev. Biol.* **2021**, *9*, 735678; b) J. O. Fuss, C.-L. Tsai, J. P. Ishida, J. A. Tainer, *Biochim. Biophys. Acta Mol. Cell Res.* **2015**, *1853*, 1253–1271.
[34] M. S. Petronek, D. R. Spitz, B. G. Allen, *Antioxidants* **2021**, *10*, 1458.

Manuscript received: June 22, 2022
Accepted manuscript online: August 25, 2022
Version of record online: September 27, 2022